RESEARCH PAPERS

J. Appl. Cryst. (1995). **28**, 369–374

Fluorescence Corrections in Thin-Film Texture Analysis

BY D. CHATEIGNER, P. GERMI AND M. PERNET

Laboratoire de Cristallographie, CNRS, associé à l'Université Joseph Fourier, BP 166, *Grenoble CEDEX* 09, *France*

AND P. FRÉCHARD AND S. ANDRIEU

*Laboratoire mixte CNRS Saint-Gobain CRPAM, UMR*37, *BP* 109, *Pont-à-Mousson CEDEX, France*

(*Received* 29 *November* 1994; *accepted* 6 *February* 1995)

Abstract

This paper reviews the transmission and reflection texture techniques in order to develop the correction formulae in each of these methods for application to fluorescent thin-film analysis. The method is applied to iron samples deposited on glass substrates in order to prove the efficiency of these corrections in the case of the Schulz reflection geometry. The columnar growth of these films is shown to be dependent on the incident flux inclination.

Introduction

In experiments using X-radiation, fluorescence emission occurs every time the atomic number of the metal constituting the target of the tube is just one or two units higher than that of an element constituting the studied material (Eberhart, 1989). Often, this effect results in an undesirable component in data processing. The effect can be avoided directly by changing the X-ray wavelength, adding a monochromator on the reflected beam or using an energy-dispersive (solid-state) detector. However, it can be inconvenient and time consuming to modify the experimental set-up to study different types of samples.

In texture-analysis experiments on bulk samples, the fluorescence effect produces an intensity level that can vary over a pole figure, depending on the diffraction line geometry. Whatever this geometry, the fluorescence component constitutes part of the defocusing curves established on a randomly oriented bulk of the same material, and consequently is subtracted from the pole-figure data when the so-called defocusing correction is applied. However, it is often impossible to produce thin films without texture, even on polycrystalline (Iijima, Tanabe, Ikeno & Kohno, 1991) or amorphous (Narumi *et al.*, 1991) substrates, since grain growth is generally anisotropic. As a result, for thin-film texture studies, we cannot use experimental curves to correct for fluorescence. We review here a method that allows us to solve this problem for transmission and reflection arrangements used in texture analysis (Bunge, 1982). These corrections allow the possibility of determining pole figures without any change in the experimental set-up. We finally apply these corrections to two samples of columnar growth of iron on glass substrate and study their textures by the Schulz reflection method (Schulz, 1949) with Cu $K\bar{\alpha}$ radiation.

Experimental

The samples were deposited by molecular-beam epitaxy. In order to achieve oblique columnar growth, a highly directive flux was induced by a Knudsen cell, in which iron was thermally evaporated in a crucible (Herman, 1982). The pressure during deposition was maintained at about 10^{-8} Pa, giving an average free path of the iron of about 10^5 m, in such a way that we can consider that no interaction occurs between atoms in the incident flux. The geometrical arrangement allows an inclination α between the incident flux $\mathbf{f}$ and the substrate normal $\mathbf{n}$ in the range [0, 80°]. Standard float-glass substrates from Saint-Gobain industries were used after being cleaned with alkaline soap in order to eliminate carbonate traces. An *in situ* pre-annealing is carried out at 373 K before deposition. The substrate and Knudsen-cell temperatures can be controlled in the ranges [273, 673 K] and [1523, 1623 K], respectively.

Texture analysis has been performed with a special goniometer consisting of a Courbon S.A. sample holder mounted in a horizontal θ–2θ goniometer. The radiation was supplied by a Rigaku RU300E rotating anode. The incident beam is monochromatized by the 002 reflection of a flat graphite crystal and collimated by two crossed slits. The diffracted beam is detected through a horizontal slit by a proportional counter. The signal is finally filtered by a single-channel analyser, transferred to a PC and processed by our own programs (*CORTEXG* and *POFINT*). We draw direct pole figures where only experimental points are represented.

Theoretical

The correction of texture-analysis data for background and defocusing effects is generally done by comparison

© 1995 International Union of Crystallography
Printed in Great Britain – all rights reserved

ISSN 0021-8898 © 1995

to random standards (Feng, 1965; Tenckhoff, 1970). This method remains available for fluorescent bulk samples without modification of the usual expressions for defocusing corrections, if the defocusing curves have been established on the same random material as the studied sample. If they have been measured on a different material (nonfluorescent bulk) or calculated, the fluorescence contribution to the pole figures has to be subtracted in a different manner. For film samples, this is always the case, since it is impossible to measure defocusing curves on perfectly untextured films. To carry out the fluorescence correction of pole figures in these two latter cases (film and bulk), we propose the following formula, giving the corrected I_c intensities from the measured I_m values for one (χ, ω) sample orientation:

$$I_c(\chi, \varphi) = K_p(\chi)[I_m(\chi, \varphi)I_{b_0} - K_b(\chi)I_{b_0} - K_f(\chi)I_{f_0}]. \quad (1)$$

χ and ω are the tilt and azimuthal angles of the sample rotations, respectively, I_{b_0} and I_{f_0} are the refined values of the background level and fluorescent signal, respectively, which appear on the θ–2θ pattern at $\chi = 0$, and $K_p(\chi)$, $K_b(\chi)$ and $K_f(\chi)$ are correction factors that take into account the variation of the corresponding intensities with the tilt angle χ. Usually, $K_p(\chi)$ and $K_b(\chi)$ are determined experimentally from the defocusing curves measured on random samples. $K_f(\chi)$ depends on the experimental configuration and is explained below. The defocusing correction factor is defined as the ratio $K_p(\chi) = [I_p(0) - I_b(0)]/[I_p(\chi) - I_b(\chi)]$, where $I_p(\chi)$ and $I_b(\chi)$ are the peak and background intensities. For thin samples, $K_p(\chi)$ has to be adequately modified from a randomly oriented bulk as described by Wenk, Sintubin, Huang, Johnson & Hove (1990) and Chateigner, Germi & Pernet (1992) for the Schulz reflection technique. The two other coefficients $K_b(\chi)$ and $K_f(\chi)$ are, respectively, equal to $I_b(\chi)/I_b(0)$ and $I_f(\chi)/I_f(0)$, where $I_f(\chi)$ is the fluorescence intensity measured at the χ angle position.

By using (1), we remove the fluorescence and background signals from $I_m(\chi, \omega)$, taking into account their χ dependence [$K_f(\chi)I_{f_0}$ and $K_b(\chi)I_{b_0}$, respectively], in order to obtain the pure diffracted peak before correcting it for peak defocusing by the $K_p(\chi)$ multiplication.

I_{b_0} and I_{f_0} refinement

Since the fluorescence signal is present at each χ position in a θ–2θ spectrum, we can estimate the two quantities I_{b_0} and I_{f_0} under the Bragg peak considered in the pole figure of interest from the θ–2θ patterns at $\chi = 0$ and $\chi > 0$ on both sides of this peak. At $\chi = 0$, the value, $y(0)$, is obtained from

$$y(0) = I_{b_0} + I_{f_0}, \quad (2)$$

while at a χ position value, $y(\chi)$ is

$$y(\chi) = I_b(\chi) + I_f(\chi) = K_b(\chi)I_{b_0} + K_f(\chi)I_{f_0}. \quad (3)$$

From (2) and (3), we deduce that

$$I_{b_0} = [y(\chi) - y(0)K_f(\chi)]/[K_b(\chi) - K_f(\chi)]. \quad (4)$$

Calculation of $K_f(\chi)$

For an elementary diffracting volume dV in the material, the incident beam, I_0, is absorbed along an incident path l_i before diffraction and fluorescence occurs in dV. Then, the exiting beams are detected after absorption along an outcoming path l_o, different from the incident one in the case of nonsymmetric geometry. While the diffracted beam is again absorbed with μ, the linear absorption coefficient, related to the monochromatic radiation employed, the fluorescence is absorbed with the coefficient μ', corresponding to (in a first approximation, with no secondary fluorescence) the most probable characteristic emission of the fluorescent element in the material, and detected in the solid angle determined by the entrance slit. The evolution of the fluorescent part of the detected signal in a typical goniometer is now examined.

Schulz reflection method

Following the work of Schulz (1949), the incident intensity on an element of thickness dt at the depth t is given by (Fig. 1)

$$dI' = \frac{I_0 G}{\sin\theta\cos\chi}\exp\left(\frac{-\mu t}{\sin\theta\cos\chi}\right)dt, \quad (5)$$

where I_0 is the total incident intensity, G is a geometrical constant that reveals the slit apertures, θ is the angle between the incident beam and the sample surface and χ is the rotation angle around the axis defined by the intersection between the sample surface and the plane (l_i, l_o). Then, dI' gives rise to the fluorescence FdI' with a constant yield F specific to the considered elements and to their atomic concentrations in the material. The fluorescence beam is absorbed along l_o with μ' and detected as the intensity dI_f:

$$dI_f = F\, dI' \exp(-\mu' t/\sin\theta\cos\chi). \quad (6)$$

The integration of (6) over the thickness of the film, T,

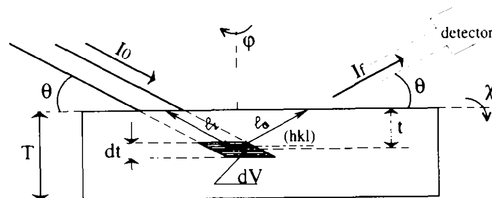

Fig. 1. Description of the Schulz symmetric reflection geometry. The co-latitude angle is denoted χ and the azimuthal angle ω. Diffracting planes are represented in the volume differential element dV.

gives the total fluorescence intensity for the position (θ, χ), which allows one to calculate the $K_f(\chi)$ factor:

$$K_f(\chi) = \frac{I_f(\chi)}{I_f(0)} = \frac{1 - \exp[-(\mu + \mu')T/(\sin\theta\cos\chi)]}{1 - \exp[-(\mu + \mu')T/\sin\theta]}. \quad (7)$$

It is interesting to notice that for bulk samples ($T \to \infty$), $K_f(\chi)$ tends to 1, *i.e.* the fluorescence signal remains constant.

Field–Merchant method

This asymmetric method (Field & Merchant, 1949) makes the sample rock around the θ position by the angle χ in the incident plane, as described in Fig. 2. The angle χ then lies in the interval $[-\theta, \theta]$, maximal values corresponding to the cut off of the incident and reflected beam, respectively, by the sample surface. In this way, χ can take positive or negative values, and for $\chi = 0$ the geometry is the same as in the Schulz method. This is also a reflection method, where the paths of the beams are related by $l_o = M(\chi)l_i$, where $M(\chi) = \sin(\theta + \chi)/\sin(\theta - \chi)$.

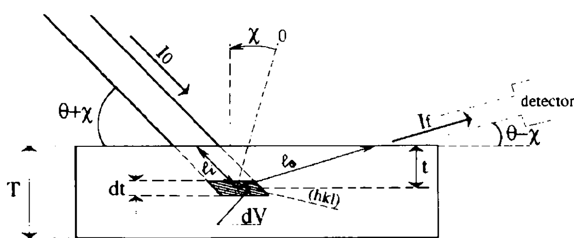

Fig. 2. Description of the Field–Merchant asymmetric reflection geometry. The rocking angle is denoted χ. This angle lies in the diffracting plane.

In a similar calculation as previously, for this geometry

$$K_f(\chi) = \left(\frac{\mu + \mu'}{\mu + M(\chi)\mu'}\right) \times \frac{1 - \exp\{-[\mu + \mu' M(\chi)]T/\sin(\theta + \chi)\}}{1 - \exp[-(\mu + \mu')T/\sin\theta]}. \quad (8)$$

For the bulk samples, (8) implies a χ dependence that takes the form $K_f(\chi) = (\mu + \mu')/[\mu + M(\chi)\mu']$. This term is a decreasing function of χ.

Decker–Asp–Harker method

In this transmission method (Decker, Asp & Harker, 1947), the θ angle is defined between I_0 and the normal to the sample surface at $\chi = 0$ (Fig. 3). The χ axis of rotation is the same as in the Field–Merchant technique with theoretical χ limits in the interval $[(\pi/2) - \theta; \theta - (\pi/2)]$, but incident and reflected beams pass successively through the film and the substrate before detection, in such a manner that

$$dI_f = dI'' \exp[-\mu_s T_s/\cos(\theta - \chi)], \quad (9)$$

where dI'' is the detected intensity for a thickness element dt at the depth t for a free sample (without substrate) and μ_s and T_s are the linear absorption coefficient and the thickness of the substrate, respectively. The exponential term reflects the absorption of the fluorescence contribution through the substrate.

Following the work of Decker, Asp & Harker (1947), and by the same reasoning as previously, one can easily obtain the expression for dI'':

$$dI'' = I_0 GF \exp(-\mu x)\exp\left[-\mu' \frac{T - x\cos(\theta + \chi)}{\cos(\theta - \chi)}\right] dx. \quad (10)$$

Here, x is the length element along the l_i path. After integration of (10) from 0 to $T/\cos(\theta + \chi)$, we obtain the

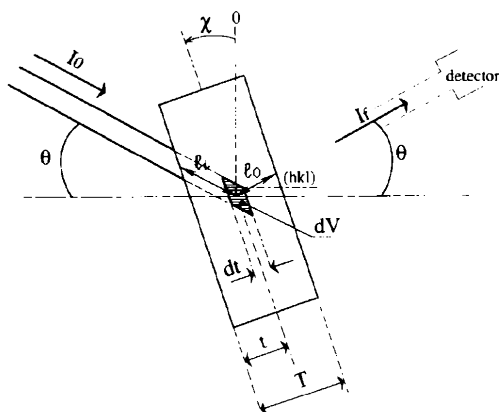

Fig. 3. Description of the Decker–Asp–Harker asymmetric transmission geometry. The rocking angle is denoted χ. The substrate is not represented here.

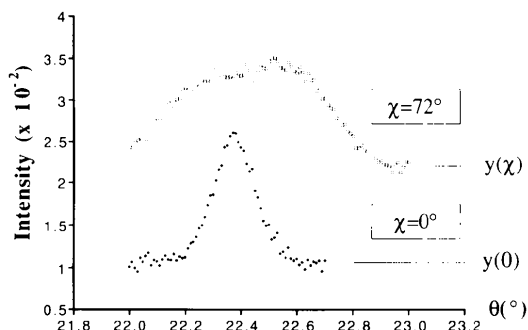

Fig. 4. θ–2θ scan of the 110 reflection of sample B, at $\chi = 0$ and $\chi = 72°$. Notice the difference in background values $y(0)$ and $y(\chi)$, which reveals the fluorescence. Integration time: 1 s.

desired ratio:

$$K_f(\chi) = \frac{b\Delta\mu}{(a\mu' - b\mu)} \frac{\exp[T(\mu'/b - \mu/a)] - 1}{\exp(T\Delta\mu/\cos\theta) - 1} \times \exp\left[\left(\frac{1}{\cos\theta} - \frac{1}{b}\right)(\mu' T + \mu_s T_s)\right], \quad (11)$$

with $\Delta\mu = \mu' - \mu$, $a = \cos(\theta + \chi)$ and $b = \cos(\theta - \chi)$.

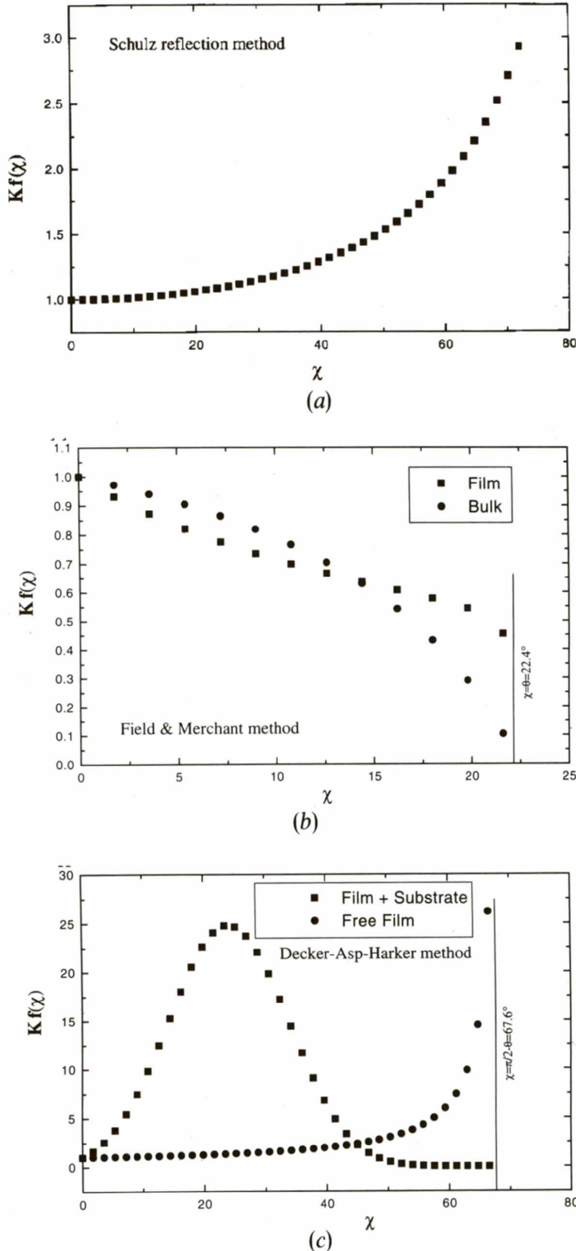

Fig. 5. $K_f(\chi)$ curves for iron samples and (110) pole figures for the three detailed geometries. (*a*) The Schulz reflection method for film *B*. (*b*) Field–Merchant geometry for film *B* (squares) and for an iron bulk (circles). (*c*) Decker–Asp–Harker geometry for films identical to that of sample *B*, when the film is free (circles) or deposited on a 150 μm thick substrate (squares) with $\mu_s = 0.12\ \mu m^{-1}$ for Fe $K\alpha$ radiation.

By checking $T_s = 0$, we obtain from (11) the evolution of the fluorescence component for free samples.

Remark on the film composition

This method of correction is applicable (without special evaluation of μ') if there is only one fluorescent element present in the material constituting the film, and if the other elements are fluorescent neither under the incident beam nor under secondary excitation. If the film contains more than one fluorescent element (with or without secondary excitation), then the fluorescent

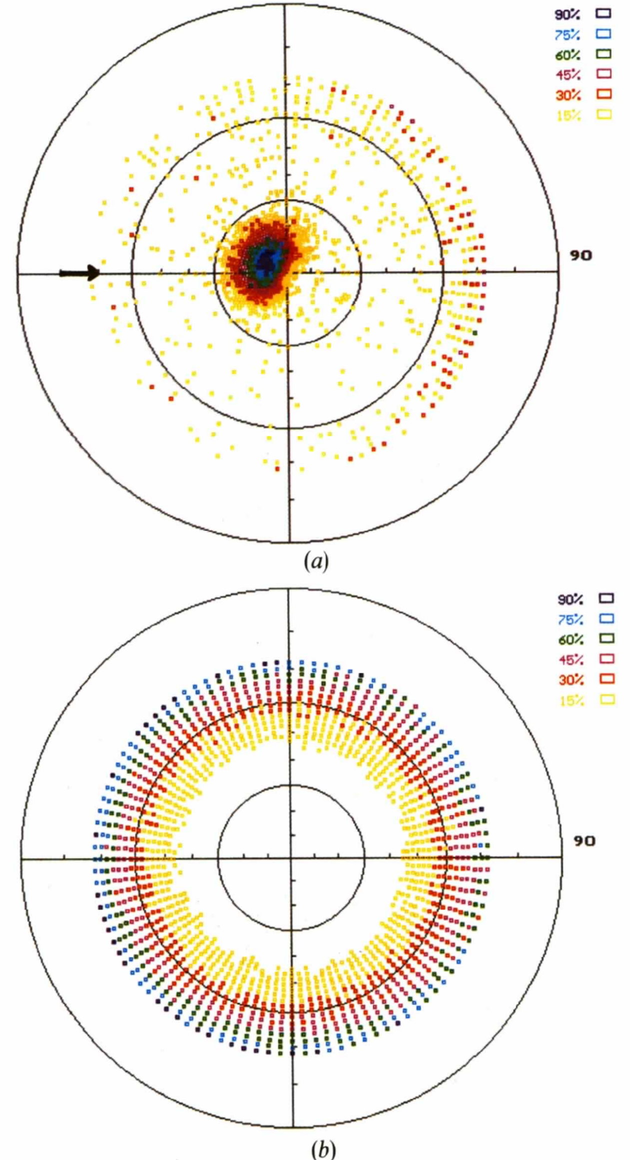

Fig. 6. (*a*) Sample *A* (200) pole figure at $\theta = 32.58°$, after correction for background, fluorescence and defocusing. We used 10 s of integration time, $\alpha = 70°$ and $T = 673$ K, and found $I_{max} = 506$ counts. (*b*) The same pole figure, but without any correction. We notice $I_{max} = 3400$ counts, at the periphery of the pole figure, entirely due to the occurrence of fluorescence.

radiation has to be analysed in detail to determine a correct equivalent μ' (with weighing over atomic concentrations and fluorescence yields).

Since the $K_f(\chi)$ curves are material dependent, specific examples of $K_f(\chi)$ calculations are given in the following section specifically for iron film and bulk.

Examples

The texture of two thin iron films (called A and B) deposited on amorphous glass substrates was analysed by the Schulz reflection technique. The film thicknesses were 300 and 1200 Å for A and B, respectively. While B was deposited under an iron incident flux (**f**) in normal incidence ($\alpha = 0°$) at ambient temperature ($T = 303$ K), the parameters $\alpha = 70°$ and $T = 673$ K were used for sample A. Iron crystallizes in cubic $Im3m$ space group with a 2.8664 Å unit-cell parameter [JCPDS (ICDD) Powder Diffraction File 6-696], absorption coefficient $\mu = 0.2426\ \mu\text{m}^{-1}$ for Cu $K\bar{\alpha}$ (1.5418 Å) and $\mu' = 0.0523\ \mu\text{m}^{-1}$ at the fluorescent Fe $K\alpha$ wavelength (1.9373 Å). We first established the two θ–2θ scans to refine the $y(0)$ (at $\chi = 0°$) and $y(\chi)$ (at $\chi = 72°$) values for the 110 and 200 reflections for both samples. An example of such a scan is presented in Fig. 4 for the 110 reflection of sample B with 1 s integration time. We observe that for this sample $y(\chi)$ is more than twice as large as $y(0)$, revealing an increase in fluorescence with an increasing irradiated volume. We can also notice the important broadening of the peak at $\chi = 72°$ due to defocusing of the beam (Gale & Griffiths, 1960).

Fig. 5 shows a calculation of $K_f(\chi)$ factors for the (110) pole figure of sample B in the three different geometries discussed in the theoretical section. In the case of the Schulz method (Fig. 5a), the calculation has been stopped at $\chi = 72°$, the limit of our pole-figure investigations. The fluorescence is very sensitive in the high-χ region.

For the Field–Merchant technique (Fig. 5b), we present for comparison $K_f(\chi)$ both for film B and an iron bulk sample. The theoretical limit of $\chi = \theta$ is indicated for the (110) pole figure by a vertical line. For film B, the fluorescence effect is compensated (compared to the bulk one) for χ values $> 15°$, because the ratio of exponential terms in (8) increases with χ. Dealing with

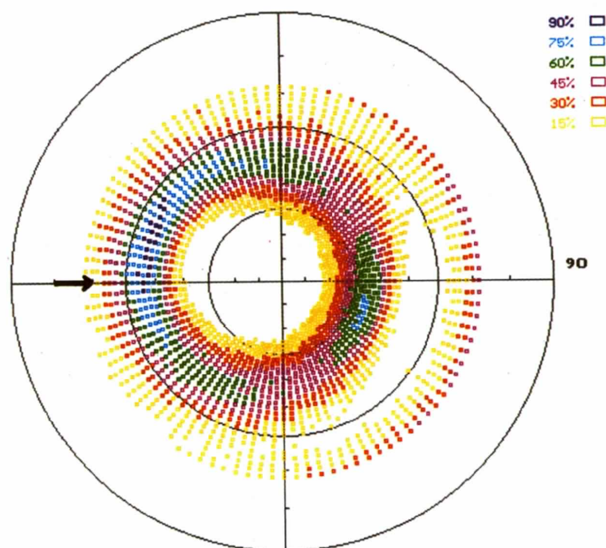

Fig. 7. Sample A (110) pole figure at $\theta = 22.4°$ with $t = 10$ s. This figure together with Fig. 6(a) confirms the (200) fibre-like texture of this sample inclined by approximately 10° from the normal towards the incident flux. $I_{max} = 2130$ counts.

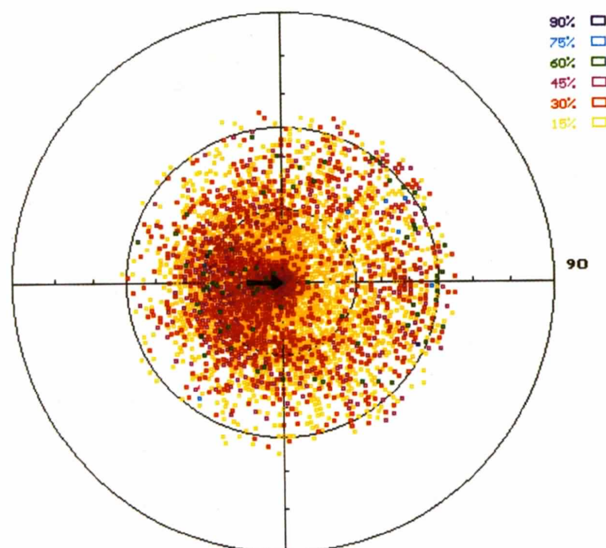

Fig. 8. Sample B (200) pole figure at $\theta = 32.58°$ with $t = 5$ s. $I_{max} = 160$ counts. The principal component is oriented close to the perpendicular to the sample plane. $\alpha = 0°$ and $T = 303$ K.

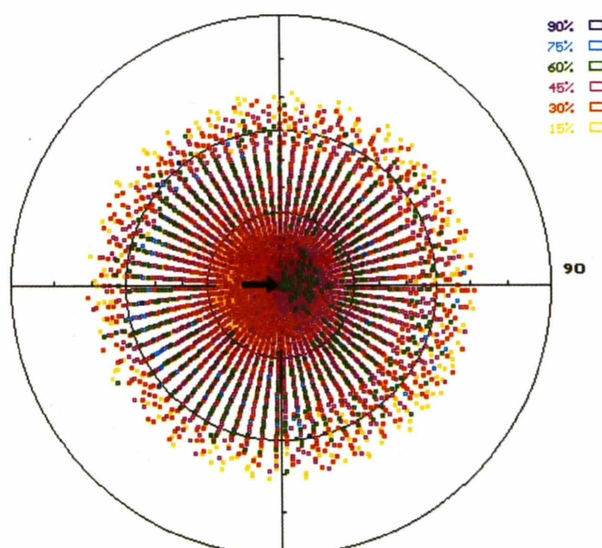

Fig. 9. Sample B (110) pole figure at $\theta = 22.4°$ for $t = 1$ s. $I_{max} = 235$ counts. Another (110) perpendicular component appears, weaker than the previous (200) one.

the Decker–Asp–Harker geometry (Fig. 5*c*), we have chosen to illustrate the $K_f(\chi)$ function for a free film (without substrate) and for a supported one. For the calculation of $K_f(\chi)$, both films have been considered identical to sample *B*, while the substrate was assumed to be 150 μm thick and to have $\mu_s = 0.12\ \mu m^{-1}$. The vertical line marks the theoretical limit, $\chi = \pi/2 - \theta$, of that method. We notice on this figure that for the free film the fluorescence signal becomes particularly important at high χ. However, for the supported film, this increase of $K_f(\chi)$ is reduced practically to zero in the same χ region by the substrate absorption. This absorption is minimum at $\chi = \theta$ where l_o is lowest, which corresponds to the maximum in the $K_f(\chi)$ curve.

We were able to analyse the corresponding (110) and (200) pole figures for which the scans were performed in the limit $0 < \chi < 72°$ with angle increments of $\Delta\chi = 1.8°$ and $\Delta\omega = 3.6°$, at $\theta = 22.4°$ and $\theta = 32.58°$, respectively. All pole figures were established at a fixed power 50 kV × 200 mA of the X-ray generator. For sample *A*, the integration time was 10 s on each measured point for all pole figures, while, for sample *B*, 1 and 5 s integration times were used, respectively, for the (110) and (200) pole figures. The **f** direction is indicated by an arrow in each pole figure. The (200) pole figure of sample *A* is shown in Fig. 6. While in Fig. 6(*a*) the correction was done with the fluorescence taken into account by the application of (1) and (7), Fig. 6(*b*) shows the (200) pole figure without any correction. It shows clearly a high-intensity ring at the 15% level as soon as χ reaches 45°, which is entirely due to the iron fluorescence. The fluorescence correction is efficient and easy to apply. This method of correction avoids any instrumental modifications. The principal concerns are the sample alignment and thickness homogeneity.

The (110) pole figure of sample *A* is presented in Fig. 7. Figs. 6(*a*) and 7 reveal a ⟨200⟩ fibre-like texture by the appearance of a ⟨110⟩ ring centred on the (200) pole, inclined by about 10° from the normal to the sample plane towards **f** and dispersed around this direction by 10° at 15% of the maximal intensity. The ⟨110⟩ ring is partially reinforced also towards **f** around $\chi = 55°$ and, of course, along the three other equivalent positions for ⟨110⟩, as a result of a weak in-plane alignment of the crystallites. On the other hand, there is a morphological tendency for the columns to be aligned with respect to **f** (Leamy, Gilmer & Dirks, 1980), well described by the empirical relation $\tan\alpha = 2\tan\beta$, where β is the angle between the substrate normal and the column axes. Using this relation with $\alpha = 70°$, we observe in sample *A* good correspondence between the calculated value of $\beta = 54°$ and the location of the crystallographic ⟨110⟩ directions at $\chi = 55°$.

The (200) and (110) pole figures of sample *B* are presented in Figs. 8 and 9, respectively. These figures demonstrate the existence of two texture components with ⟨110⟩ and ⟨200⟩ directions both perpendicular to the sample plane. By the examination of the relative intensity levels we can say that the ⟨200⟩ texture is dominant, but is more extended than in sample *A*. We can also notice that a relatively large proportion of the crystallites are randomly oriented. These two latter facts seem to be the result of a lower deposition temperature and will be the subject of future work.

Concluding remarks

We have derived a new method for correcting pole figures for fluorescent signals in the three principal geometries used in thin-film analysis. These corrections have been proven efficient and easy to apply in the case of texture analysis of iron films, using the Schulz reflection geometry. A film as thin as 300 Å has been successfully studied without particular problems using our experimental set-up. The case of multifluorescent elements has not been tested but seems to be tractable if secondary fluorescence does not take place.

In the case of columnar iron films, we have shown that it becomes possible to correlate the morphology and the crystallographic directions of the columns.

References

Bunge, H. J. (1982). *Quantitative Texture Analysis*, edited by H. J. Bunge & C. Esling, p. 85. Deutsche Gesellschaft für Metallkunde EV, Germany.

Chateigner, D., Germi, P. & Pernet, M. (1992). *J. Appl. Cryst.* **25**, 766–769.

Decker, B. F., Asp, E. T. & Harker, D. (1947). *J. Appl. Phys.* **19**, 388–392.

Eberhart, J. P. (1989). *Analyse Structurale et Chimique des Matériaux*, p. 319. France: Dunod.

Feng, C. (1965). *J. Appl. Phys.* **36**, 3432–3435.

Field, M. & Merchant, M. E. (1949). *J. Appl. Phys.* **20**, 741–745.

Gale, B. & Griffiths, D. (1960). *Br. J. Appl. Phys.* **11**, 96–102.

Herman, M. A., (1982). *Vacuum*, **32**, 555–565.

Iijima, Y., Tanabe, N., Ikeno, Y. & Kohno, O. (1991). *Physica (Utrecht)*, C**185–189**, 1959–1960.

Leamy, H. J., Gilmer, G. H. & Dirks, A. G. (1980). *Curr. Top. Mater. Sci.* **6**, 309–344.

Narumi, E., Song, L., Li, C., Kao, Y. H., Patel, S., Shaw, D. T., Shue, S. & Fujino, K. (1991). *Jpn. J. Appl. Phys.* **30**, L585–L586.

Schulz, L. G. (1949). *J. Appl. Phys.* **20**, 1030–1033.

Tenckhoff, E. (1970). *J. Appl. Phys.* **41**, 3944–3948.

Wenk, H. R., Sintubin, M., Huang, J., Johnson, G. C. & Hove, R. T. (1990). *J. Appl. Phys.* **67**, 572–574.